ELSEVIER

Atmospheric Research 73 (2005) 131–148

ATMOSPHERIC RESEARCH

www.elsevier.com/locate/atmos

Effects of arctic sulphuric acid aerosols on wintertime low-level atmospheric ice crystals, humidity and temperature at Alert, Nunavut

Eric Girard*, Jean-Pierre Blanchet, Yves Dubois

Department of Earth and Atmospheric Sciences, University of Quebec at Montreal, Montreal, QC, Canada H3X 2H9

Received 17 November 2003; received in revised form 18 August 2004; accepted 24 August 2004

Abstract

The effect of pollution-derived sulphuric acid aerosols on wintertime arctic lower atmospheric ice crystals is investigated. These anthropogenic aerosols differ from natural background aerosols by their number concentration, strong solubility and reduced homogeneous freezing temperature when internally mixed with other compounds. Furthermore, observations suggest that the ice-forming nuclei concentration is reduced by one to four orders of magnitude when the sulphuric acid aerosol concentration is high.

Simulations performed using a column model and analysis of observed data for the period of 1991–1994 at Alert (82° 30'N, 62°20'W) are used to assess the changes of the boundary layer cloud characteristics by sulphuric acid aerosols and the potential effect on arctic climate. Results show that aerosol acidification leads to depletion of the ice crystal number concentration and an increase of its mean size. As a result, low-level precipitating ice crystals occur more frequently than ice fog and thick nonprecipitating clouds during high concentration of pollution-derived aerosols. This result is in agreement with observations that indicate an increase by more than 50% of the frequency of precipitating ice crystals when the weight proportion of sulphuric acid is greater than its mean value of 20% of the total aerosol mass. Consequently, the ice crystal size increases and number decreases, and the sedimentation flux of ice crystals and the dehydration rate of the lower troposphere are accelerated in the presence of high sulphuric acid aerosol concentration. As a result, the infrared radiation flux reaching the surface and the greenhouse effect are decreased. This process is referred

* Corresponding author. Tel.: +1 514 987 3000x3325; fax: +1 514 987 7749.
E-mail address: girard.eric@uqam.ca (E. Girard).

0169-8095/$ - see front matter © 2004 Elsevier B.V. All rights reserved.
doi:10.1016/j.atmosres.2004.08.002

to as the dehydration–greenhouse feedback. One-dimensional simulation for Alert during the period of 1991 to 1994 shows that a negative cloud radiative forcing of -9 W m^{-2} may occur locally as a result of the enhanced dehydration rate produced by the aerosol acidity.
© 2004 Elsevier B.V. All rights reserved.

Keywords: Aerosols; Climate; Arctic; Clouds

1. Introduction

Lower tropospheric ice crystal events are common in the Arctic during the cold season, from November to May (Curry et al., 1990). Depending on the ice crystal concentration in the air and the associated visibility, these events occur as either diamond dust or ice fog. Observations show a frequency up to 50% for diamond dust and around 10% for ice fog during the cold season (Maxwell, 1982; Curry et al., 1990; Girard and Blanchet, 2001b). Due to the difficulties of observing these events, their frequency may be even higher than reported by meteorological stations and indicated by satellite imagery analysis (Curry et al., 1990).

During the cold season, synoptic systems that form in the strong baroclinic zone in the Northern Hemisphere regularly inject mild and moist air to the Arctic. The absence of solar radiation leads to rapid infrared cooling of the surface. The surface cooling progressively spreads upward, and ultimately, the warm and moist air mass is transformed to cold and dry arctic air mass. In the process of cooling, air becomes supersaturated with respect to ice and ice crystals nucleate. Observations (Wexler, 1936) and modelling (Curry, 1983; Girard, 1998) have shown that the air mass transformation takes about 2 weeks to reach typical arctic air temperatures. The arctic air mass formation depletes the lower atmosphere of its internal energy via infrared cooling but increases its available potential energy. Dynamically, at large scale, the internal energy deficit in the Arctic leads to an intensification of baroclinic instabilities, which in turn perturb large-scale circulation through cyclogenesis. Energy balance between the pole and lower latitudes is then achieved by the new injection of mild and moist air from mid-latitude synoptic systems. The enhanced circulation further promotes the transport of pollutants into the Arctic. Therefore, not only there is a local feedback between dehydration and infrared radiation but also between synoptic circulation and pollution injection. The injection is maximum in the lower troposphere between 700 and 900 hPa. The Arctic wide infrared cooling of mild, moist and polluted air injected from mid-latitudes is probably the main source of widespread and continuous formation of ice crystals in the Arctic lower atmosphere (Curry et al., 1990).

To our knowledge, no quantitative definition of diamond dust and ice fog exists. A quantitative definition of diamond dust and ice fog can be suggested based on observations (Curry et al., 1990 for a comprehensive review) and modelling (Girard and Blanchet, 2001a,b). In this paper, a diamond dust event is defined as a cloud with ice crystal concentration below 1000 l^{-1} and crystal size larger than 30-μm diameter forming in the boundary layer and slowly precipitating to the ground. Ice crystals precipitating from thin liquid or mixed-phase clouds are also considered to be diamond dust as long as they meet

the diameter and concentration threshold cited above. In this paper, diamond dust and low-level precipitating ice crystals from thin boundary layer liquid clouds will be called low-level ice crystals (LLIC). Ice fog is defined as a cloud composed of ice crystals that form just above the ground, having concentration exceeding 1000 l^{-1} with diameter below 30 μm. While LLIC particles have a significant deposition velocity, ice fog particles are generally too small and usually remain in suspension in the atmosphere. Ice fog dissipates radiatively by either mixing with warmer air or by heating from solar radiation.

Observations (Curry et al., 1990) and modelling (Curry, 1983; Blanchet and Girard, 1995; Girard and Blanchet, 2001a) have shown that LLIC contribute substantially to the net radiation balance during the cold season (from November to May). Using observed temperature and ice crystal concentration from Witt (1968) during December 1968 in Alaska and Arctic gas and aerosol sampling program (AGASP) observations in spring of 1983 and 1986 (Schnell, 1984) as inputs for a radiative model, Curry et al. (1990) found that LLIC can contribute to the surface radiative flux nearly 80 W m^{-2} during winter and up to 15 W m^{-2} during spring (positive values for heating). Using a time-dependent single-column model, Blanchet and Girard (1995) estimated the radiative contribution of LLIC by comparing two 2-day infrared air mass cooling with and without the ice crystal radiative contribution. Results showed a surface warming of 10 °C in 48 h due to ice crystal formation in the lower atmosphere. Using an explicit aerosol and cloud microphysics radiation coupled model designed to simulate arctic LLIC and ice fog, Girard and Blanchet (2001a) obtained an increase up to 60 W m^{-2} of the downward infrared flux at the surface during winter due to "mixed phase" diamond dust (which is defined here as ice crystals precipitating from thin boundary layer liquid cloud) and ice fog. The SHEBA field experiment showed that LLIC is often accompanied with low thin liquid clouds at the top of the surface-based temperature inversion (Intrieri and Shupe, 2004). The contribution of these clouds to the surface radiative budget during SHEBA was substantial with values up to 40 W m^{-2}.

Following ice crystal formation and sedimentation, water vapour is depleted in the lower troposphere. This cold drying effect is a dominant dehydration process in the Arctic. It is known that water vapour is by far the strongest greenhouse gas in the atmosphere. At low temperatures typical of the Arctic during winter, due to the rapid decrease of water vapour optical depth in the rotation band and shifting of the plank function maximum toward lower frequencies, water vapour becomes more sensitive to temperature and moisture depletion in the Arctic than at lower latitude regions. Fig. 1 shows that in cold arctic conditions, the greenhouse forcing is a highly nonlinear function of temperature as seen by the systematic shift in the curves and the strong erosion of water vapour emissivity in the rotation band. At tropopause temperatures, the rapid collapse of the water vapour lines is highly sensitive to the air mass dehydration rate. During winter, these conditions occasionally reach the surface. As a result, the arctic surface radiative budget becomes very sensitive to the alteration of the water vapour mixing ratio (Blanchet and Girard, 1995; Curry et al., 1995).

According to Curry et al. (1996), aerosols acting as condensation and deposition nuclei can have a significant impact on the ice crystal formation process. An indirect radiative forcing can occur from variation of humidity, aerosol properties and ice crystal mean diameter and concentration. Observations (Bigg, 1980; Barrie, 1986; Shaw, 1995; Yli-

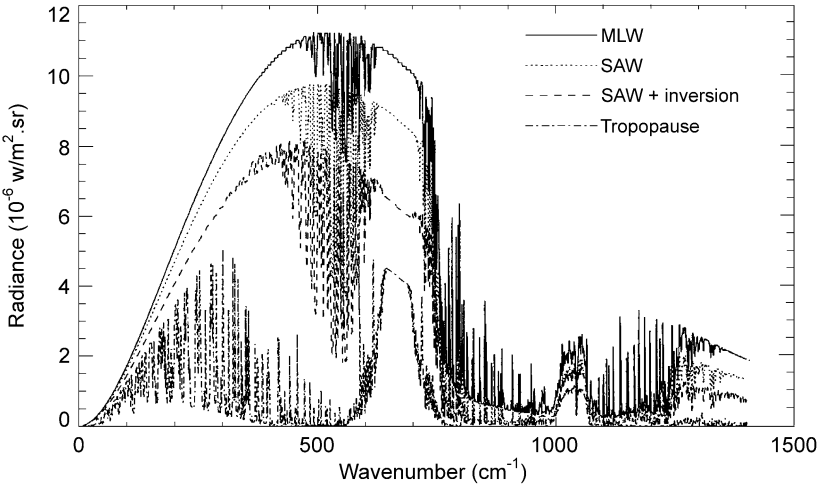

Fig. 1. Downward spectral radiance at the surface level calculated with MODTRAN for an incident angle of 53° and for three different atmospheric temperature profiles: standard mid-latitude winter (MLW), sub-arctic winter (SAW), sub-arctic winter with a −20 °C surface inversion in the lower kilometre. The last curve represents the radiance at the tropopause level in SAW conditions.

Tuomi et al., 2003) showed that anthropogenic sulphuric acid covers nearly all aerosol particles on a large scale during the cold season in the Arctic. A lower concentration of ice nuclei is often associated with high concentration of acidic aerosols. Measurements by Borys (1989) over the Arctic in April 1986 showed that the ice nuclei (IN) concentration is one to four orders of magnitude lower in polluted arctic haze as compared to cleaner nonhaze events. Bigg (1996) also observed much lower IN concentration in the Arctic when compared to mid-latitude IN concentrations. Although anthropogenic sulphuric acid aerosols are dominant in the arctic winter polluted troposphere, other natural background aerosols, among which some are good IN such as soil particles and organic compounds (Szyrmer and Zawadzki, 1997), are also reported (Barrie, 1986). The decrease of IN concentration when sulphuric acid aerosol concentration increases is still unexplained. It is a subject of ongoing research. Borys (1989) hypothesized that the concentration of ice deposition nuclei might be reduced by condensation and coagulation with sulphuric acid aerosols during their long-range transport to the Arctic. The resulting particles are composed of an internal mixing of the original components with the addition of a liquid sulphuric acid coating that inhibits ice formation by water vapour deposition. Although this hypothesis could explain the reduction of ice crystal nucleation by deposition and contact modes, it does not explain the decrease of other ice nucleation processes such as immersion and condensation freezing. Further research is needed to fully explain these observations.

Homogeneous freezing of interstitial haze particles is thought to be a major formation process of ice fog during winter at temperatures below −38 °C. The lack of IN at very low temperature makes possible the homogeneous freezing of inactivated haze submicron droplets in the Arctic during winter. The homogeneous freezing temperature of acid

particles is strongly modified by the weight fraction of acid in the particles (Bertram et al., 1996; Koop et al., 1998). In laboratory experiments, they found that the homogeneous freezing temperature is depressed by as much as 5 °C when a particle contains only 10% by weight of sulphuric acid. The decreasing rate of the homogeneous freezing temperature dramatically increases for higher values of acid concentration, making the homogeneous freezing of sulphuric haze droplets very unlikely.

Based on arguments of low ice nucleation ability mentioned above, Blanchet and Girard (1994, 1995) hypothesized that pollution-derived acid aerosols would result in the formation of fewer and larger ice crystals. As a result, the terminal velocity and the precipitation rate of ice crystals increase, and the dehydration rate of the lower troposphere is enhanced. The net radiative effect of accelerated dehydration would be a decrease of the downward infrared radiation to the surface and a strengthening of the low-level temperature inversion. In turn, surface cooling spreading into the planetary boundary layer can increase the dehydration rate, establishing a feedback between greenhouse radiative forcing and dehydration. Furthermore, the decrease of ice nucleus number concentration self-protects existing aerosols by the inhibition of ice formation and helps to maintain a high pollution level in the arctic atmosphere. This is the branch of this complex cycle that is addressed in this paper. Its confirmation and the evaluation of its strength would promote the importance of studying further the microphysical processes.

This feedback process, acting on each cycle of air mass transformation, would give rise to measurable effects on the lower troposphere and surface temperature at seasonal and climatological time scales. We refer to this mechanism as the dehydration–greenhouse feedback (Blanchet and Girard, 1994, 1995).

In this paper, the hypothesis of Blanchet and Girard (1994, 1995) is further addressed. The effect of aerosol acidification on ice crystals, humidity and temperature is evaluated using a single-column model and corresponding observations. Section 2 describes the model. Results are analyzed and discussed in Section 3.

2. Models

To evaluate the impact of aerosol acidification on the lower ice crystal and humidity, the local climate model (LCM; Girard and Blanchet, 2001b), is used to perform simulations of several winter seasons. Using observed aerosol composition and concentration, the LCM allows for a more realistic sensitivity study of the impact of aerosol composition on cloud formation and evolution on a longer time scale than the full 3D version GCM.

The LCM is the single-column version of the Northern aerosol regional climate model (NARCM; Gong et al., 1997a). The model has 49 vertical levels with 26 levels between 900 hPa and the surface allowing for high-resolution simulation of the vertical structure of the boundary layer. The explicit aerosol representation and an innovative method to retrieve dynamics tendencies using observations, the residual iterative method (RIM; Girard and Blanchet, 2001b) constitute its uniqueness from other similar type models (e.g., see Randall and Cripe, 1999). The cloud microphysics scheme developed by Girard and Blanchet (2001b) describes clouds with four prognostic variables: the mean diameter and

the mixing ratio of ice crystals and water droplets. A bimodal shape of the cloud particle size distribution is assumed. Each mode represents water or ice phases. The aerosols are represented by eight size bins from 0.01 μm to 2 μm allowing for prognostic and explicit simulation of the aerosol spectrum. Coagulation, wet and dry deposition are the aerosol physical processes simulated by the LCM. Coalescence, aggregation, condensation, deposition, sublimation, evaporation, gravitational deposition and homogeneous and heterogeneous freezing are represented in the model.

A detailed description of the aerosol and cloud parameterisations is given by Gong et al. (1997a) and Girard and Blanchet (2001a,b), respectively. The physical processes that are not related to aerosols and clouds are from the Canadian GCM (McFarlane et al., 1992).

Inasmuch as the parameterisation of the ice nucleation process has been substantially modified compared to the former version of the microphysics scheme (Girard and Blanchet, 2001b), a brief description is given here. In this paper, homogeneous freezing means the nucleation of ice from liquid phase without the help of solid aerosol particles while heterogeneous nucleation of ice occurs onto a solid aerosol particle, the so-called ice nucleus, which facilitates the ice nucleation process.

Homogeneous freezing of haze droplets depends on their composition. Thus far, only ammonium sulphate and sulphuric acid haze droplets are considered in the model for homogeneous freezing. Organics, which contribute substantially to the total aerosol mass in the accumulation mode, may also have significant effect but are neglected due to their very complex nature and lack of knowledge regarding their freezing properties. When other components such as organics, sea salt and soil particles are internally mixed with ammonium sulphate or sulphuric acid aerosols, it is assumed that they have no effect whatsoever on the homogeneous freezing temperature other than decreasing the percentage by weight of either ammonium sulphate or sulphuric acid. The homogeneous freezing temperature of ammonium sulphate haze droplets (T_{NH4SO4}) in Kelvin is parameterised according to laboratory experiment of Cziczo and Abbatt (1999):

$$T_{(\mathrm{NH_4})_2\mathrm{SO_4}} = a_0 + a_1 m_{(\mathrm{NH_4})_2\mathrm{SO_4}} + a_2 m^2_{(\mathrm{NH_4})_2\mathrm{SO_4}}$$

where a_0=235.15, a_1=−0,2473, a_2=0.007 and $m_{(\mathrm{NH4})2\mathrm{SO4}}$ is the percentage by weight of ammonium sulphate in haze droplets. Note that the size bin representation of aerosols allows for variable homogeneous freezing temperatures for haze droplets as a function of particle sizes. The treatment of the temporal variability of the saturation ratio within a time step is described in Girard and Blanchet (2001a,b)). The maximum value of the saturation ratio reached within a time step is used to calculate the percentage by weight of ammonium sulphate in haze droplets. The homogeneous freezing temperature of sulphuric acid haze droplets (T_{H2SO4}) is determined using Koop et al. (1998) laboratory experiment:

$$T_{\mathrm{H_2SO_4}} = A_0 + A_1 m_{\mathrm{H_2SO_4}} + A_2 m^4_{\mathrm{H_2SO_4}} + A_3 \exp(m_{\mathrm{H_2SO_4}})$$

where A_0=235,28, A_1=−0.81592, A_2=-5.8949×10^{-5}, A_3=-2.0021×10^{-11}, and m_{H2SO4} is the percentage by weight of sulphuric acid in haze droplets.

Heterogeneous ice nucleation by the condensation freezing, contact and deposition modes is treated using the parameterisation of Meyers et al. (1992). Immersion freezing depends on temperature and droplet volume, following Bigg (1953). A modified version

of the parameterisation of heterogeneous ice nucleation is also introduced in the model to account for the reduction of ice nucleus concentration in the presence of sulphuric acid aerosols. Observations by Borys (1989) have been used along with aerosol observation at Alert to derive an expression for the reduction of IN as a function of percentage by weight of sulphuric acid in aerosols. To adjust the scale, we assume that the maximum percentage by weight of sulphuric acid observed at Alert corresponds to the maximum IN reduction observed by Borys (1989). In the case of Alert, it represents a reduction of four orders of magnitude of IN concentration when the percentage by weight of sulphuric acid is 46%. For other concentrations of sulphuric acid, the following relationship has been derived for the factor of reduction of IN, F_R:

$$F_R = 10^{8.67 m_{H_2SO_4}}$$

where m_{H2SO4} is the percentage by weight of H_2SO_4. Inasmuch as aerosol composition was not observed by Borys, this relationship is based on three hypotheses: (1) the range of percentage by weight of sulphuric acid observed at Alert is similar to that of the air mass sampled by Borys; (2) sulphuric acid is responsible for the reduction of IN concentration observed by Borys; and (3) IN concentration decreases exponentially with H_2SO_4 concentration, allowing for a small perturbation at low sulphuric acid concentration. These hypothesis need to be further verified by future field and laboratory experiments. However, for sensitivity process studies, it is reasonable to make these assumptions given limited observations available and the intent to remain within realistic parameters.

3. Results

Aerological soundings plus aerosol composition and concentration observed (10 m above the ground) at Alert from 1991 to 1994 are used for simulations. These data allow inferring the residual dynamics tendencies for momentum, humidity, temperature, in addition to aerosol size and concentration, through the residual iterative method (RIM). The description of this method and its application to the case simulated in this study is discussed by Girard and Blanchet (2001b). Aerological soundings provide vertical profiles of temperature, humidity and winds twice a day, at 0000 and 1200 UTC. Aerosol observations were taken 6 km south of the main base on an elevated plateau 210 m above sea level (Sirois and Barrie, 1999). Aerosol concentrations and types are available once a week near the surface only. The model is initialized with the observed aerosol concentration and composition. Although concentration and composition of aerosols are given, their vertical and size distributions are not available from observations.

In this model, the shape of the aerosol size distribution is prognostic. However, we initialize the model with a bimodal lognormal size distribution having maxima centred at 0.17 μm and 0.6 μm and standard deviations of 1.42 and 2.01 for the accumulation mode and giant mode, respectively. This initial aerosol size distribution is the same as used by Blanchet and List (1987) who determined these parameters with the observations of Bigg (1980) and Heintzenberg (1980). These parameters are quite representative of many other observations showing the characteristic narrow aerosol bimodal size distribution (Pueschel et al., 1986; Trivett et al., 1988; Radke et al., 1989). Initially, the aerosol mass is divided

between each mode according to the relative aerosol composition. Sulphate, soot, organics and other trace substances like metals compose the accumulation mode. It is assumed that sea salt and soil particles are confined to the giant mode. After initialization, the explicit aerosol microphysics of the LCM simulates explicitly the subsequent evolution of the aerosol spectra at each level. Weekly aerosol observations are used to assimilate the aerosol dynamics tendency using the RIM procedure.

The observed aerosol composition is used to determine tendencies of the aerosol mass concentration of the accumulation and giant modes. It is also used to determine the homogeneous freezing temperature of haze particles, the ice forming nuclei concentration and the hygroscopic growth of aerosols. Inasmuch as aerosol observations are available only at the surface, we assume a constant aerosol composition in the vertical up to 200 hPa. Above 200 hPa, no implication of aerosols is considered. An idealized vertical profile for aerosol concentration is assumed with the largest concentration near the surface decreasing linearly with height.

The assumption of constant aerosol composition may appear in contradiction with several observations that indicate important variations in the vertical (Schnell and Raatz, 1984; Shaw, 1995). However, there is no common denominator between observations with regard to the aerosol vertical structure in the Arctic. It generally depends on the presence of clouds and on the air layer origin, which vary as a function of the height (Shaw, 1995). In fact, arctic haze often appears in sharp layers at different heights. This is due to the fact that anthropogenic aerosols follow nearly isentropic surfaces from source regions to the Arctic. Consequently, it is a simpler and unambiguous choice to assume a uniform vertical structure of aerosol composition in the absence of measurements. Despite this limitation, Girard and Blanchet (2001b) have shown that the LCM is capable of reproducing reasonably well the mean value and the standard deviation of LLIC and ice fog weekly frequency (weekly frequency is calculated based on hourly observations) with this assumption of a uniform aerosol composition in the vertical. Inasmuch as we analyze relative changes, we expect no excessive error due to this limitation. Our prime objective is to capture the variability of air mass characteristics and corresponding aerosol mass concentration and acidic content. In our conclusions, we will account for this assumption. The simulation of the vertical structure will be addressed in a future 3D experiment.

Simulations of four cold seasons, from November 1st to April 30th, over the period of 1991 to 1994 were performed. Table 1 shows the three aerosol scenarios that were compared: scenario A in which all the sulphate is assumed to be ammonium sulphate; scenario B representing the observed aerosol composition at Alert, that is, a pollution-

Table 1
Aerosol scenarios used in the simulations

	Scenario A	Scenario B	Scenario C
Aerosol composition	100% Ammonium sulphate	As observed	100% Sulphuric acid
Homogeneous freezing temperature of haze droplets	Cziczo and Abbatt (1999)	Koop et al. (1998)	Koop et al. (1998)
Ice nuclei (IN) concentration	Meyers et al. (1992) (F_r=1.)	Meyers et al. (1992) reduced by a factor F_r (F_r=$^{108.67sw}$)	Meyers et al. (1992) reduced by four orders of magnitude (F_r=0.0001)

derived aerosols scenario dominated by sulphuric acid aerosols during winter and ammonium sulphate aerosols during autumn; scenario C representing an extreme acidic case in which all aerosol are assumed to be coated by pure sulphuric acid only. In the latter case, a prescribed reduction of the ice forming nucleus concentration of four orders of magnitude is imposed (F_r=0.0001). In anthropogenic scenario B, the reduction of the IFN concentration depends on the mass ratio between sulphuric acid and total aerosol (variable F_r). The averaged proportion of total sulphate serving for the formation of sulphuric acid aerosols varies from 10% in early autumn to a maximum of about 50% during spring. The homogeneous freezing temperature of haze droplets is based on Koop et al. relationship in scenarios B and C.

Scenario A is the baseline simulation. Therefore, dynamics tendencies are calculated using RIM based on scenario A and applied to all scenarios equally. This is equivalent to assuming that the aerosols have no effect on atmospheric circulation. The goal is to isolate the effect of aerosol acidification on cloud and radiation through local thermodynamical process only. The subsequent feedbacks through a circulation process resulting from alteration of cloud properties due to sulphuric acid aerosols in scenarios B and C need to be done in full 3D simulations. At this stage of our investigation, the focus is placed on better understanding the complex thermodynamic processes involved in the interaction between acidic aerosol, cloud, radiation and precipitation. Understanding local processes is a prerequisite for the interpretation and the analysis of full 3D simulations that accounts also for dynamical feedbacks.

Table 2 shows the frequency of low-level precipitating ice crystals, ice fog and cloud amount simulated by the three scenarios. When compared to scenarios A and C, scenario B better reproduces observed low-level precipitating ice crystal frequency. Cloud amount is reasonably well captured by scenarios A and B with values of 0.58 and 0.41, respectively, as compared to an observed value of 0.50. Scenario C underestimates cloud amount. Ice fog frequency is very low in all three scenarios with values below 0.02 as compared to 0.11 for observations. These results suggest that aerosol acidification increases low-level precipitating ice crystal events in the lower troposphere and decreases cloud amount in the troposphere. In these simulations, the assumption of constant aerosol properties in the vertical is likely to lead to an overestimation of aerosol acidity in the troposphere. As a result, cloud amount is slightly underestimated in scenario B. Field experiments such as AGASP have shown that arctic haze is generally confined within several thin atmospheric layers in the lower 5 km of the troposphere. This suggests that the mean aerosol acidity in the boundary layer is likely to be overestimated in our simulations. Ice fog events depend on both temperature and aerosol microphysical properties.

Table 2
Cloud amount, ice fog and clear sky ice crystal precipitation frequencies simulated by the model with three aerosol scenarios and observed values

	Scenario A	Scenario B	Scenario C	Observations
Cloud amount	57.5	41.1	1.2	50.0
Ice fog frequency	1.6	1.6	1.5	11.0
Clear sky precipitation frequency	19.7	23.0	39.3	26.0

Cloud amount is the frequency multiplied by cloud cover.

Temperature in the boundary layer is rarely cold enough for ice fog formation. Observed ice fog events might be enhanced by high IN concentration in the nearby area and advected over the observation site. Rogers et al. (2001) reported this phenomenon during the SHEBA experiment with IN concentration reaching 1000 l^{-1} at 2% water supersaturation.

Fig. 2 shows vertical profiles of (a) ice crystal mean diameter, (b) ice crystal number concentration and (c) saturation ratio averaged over the four cold seasons for the three aerosol scenarios simulated by the model. The effect of aerosol acidification on cloud microphysics through ice nucleation is evaluated by comparing scenarios B and C with scenario A.

In the acidic scenarios, the ice crystal mean diameter is generally larger with a maximum increase of a factor 3 in the upper atmosphere in scenario C. Fig. 2a shows that the increase of the mean diameter due to aerosol acidification in the lower troposphere is around 25% for both scenarios except very close to the surface where the differences are small. Ice crystal number concentration is reduced by several orders of magnitude in scenario C when compared to scenario A (see Fig. 2b). In scenario B, the ice crystal number concentration is significantly reduced in the layer 800–950 hPa when compared to scenario A. Fig. 2c shows that the mean ice saturation ratio increases substantially in scenario C whereas scenario B remains close to the natural case.

Two factors associated to the increase of the acid concentration contribute to this result: a lower homogeneous freezing temperature of haze droplets and a decrease of the IN concentration. The lowering of the homogeneous freezing temperature for interstitial acid aerosols is a dominant factor contributing to increased mean cloud particle size. Indeed, the temperature has to reach several degrees below −40 °C for the homogeneous freezing occurrence. According to Walsh and Chapman (1998), such low temperatures seldom occur in the lower troposphere. This favors LLIC formation at the expense of ice fog or clouds. Table 2 shows that LLIC frequency is higher in scenarios B and C as compared to scenario A. The homogeneous freezing temperature depression also affects cloud formation in elevated layers where temperatures are often below −40 °C. Table 2 shows also that cloud amount is much reduced in the pure acid scenario C as compared to more realistic scenarios A and B. This is due to the fact that, in this scenario, the homogeneous freezing temperature is rarely reached due to high percentage by weight of sulphuric acid of the haze particles (all aerosols are assumed to be sulphuric acid in this scenario). The decrease of cloud amount is much smaller in scenario B due to the temporal variability of sulphuric acid mass fraction in aerosols. Indeed, as the proportion of sulphuric acid decreases, homogeneous freezing occurs and upper clouds form quickly. This situation can lead occasionally to the formation of clouds having high ice crystal number concentration owing to the increase of aerosol mass concentration in the accumulation mode during previous episodes of high acidic concentration in the aerosols. On average, the depression of homogeneous freezing temperature for acidic haze droplets increases the LLIC frequency and decreases the cloud amount.

Fig. 2. Vertical profile of (a) ice crystal diameter, (b) number concentration of ice crystals and (c) saturation ratio with respect to ice; averaged over the four cold seasons simulated by the model for three aerosol scenarios: scenario A (full line), scenario B (dotted line) and scenario C (dashed line).

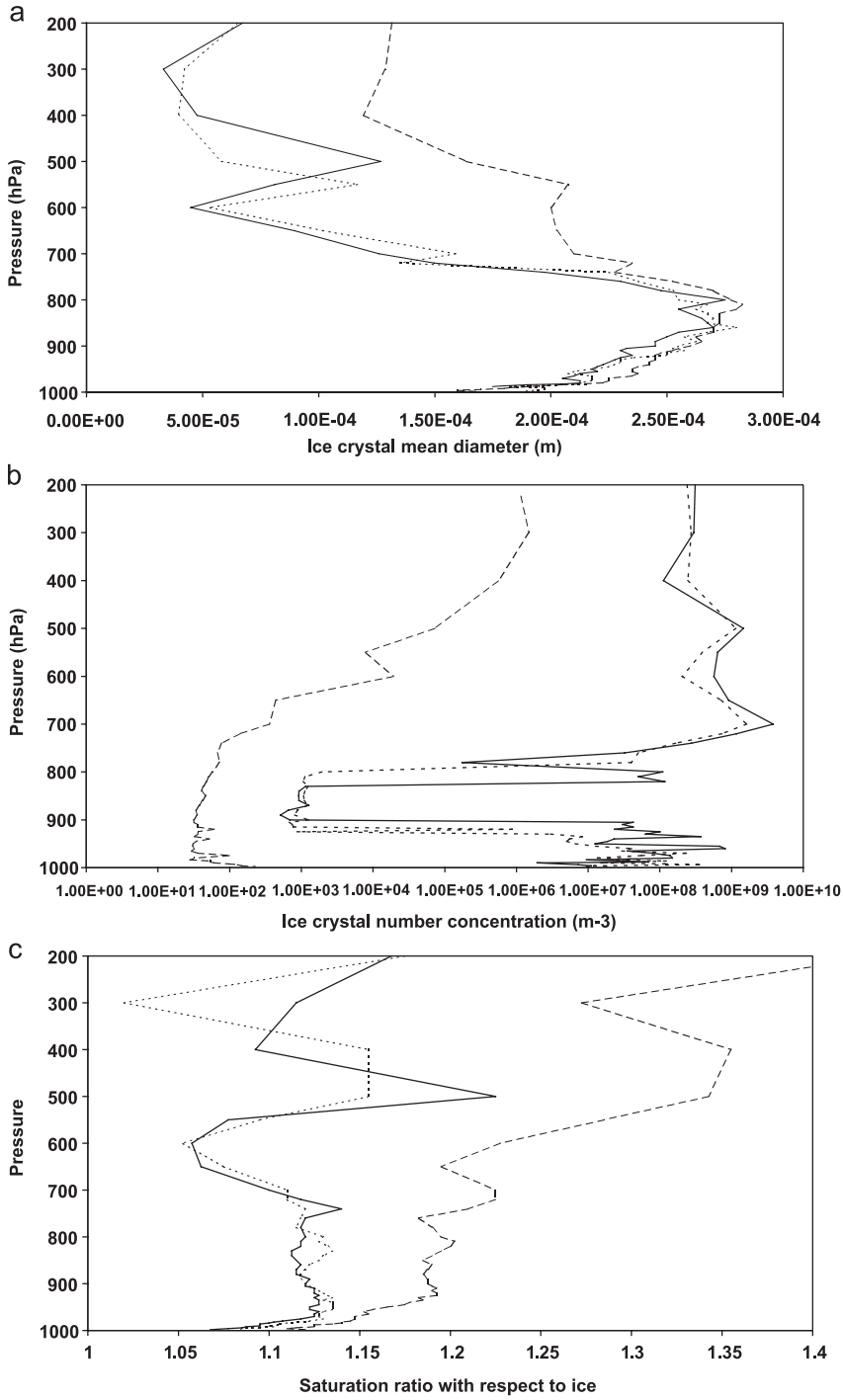
a
Pressure (hPa)
200
300
400
500
600
700
800
900
1000
0.00E+00
5.00E-05
1.00E-04
1.50E-04
2.00E-04
2.50E-04
3.00E-04
Ice crystal mean diameter (m)
b
Pressure (hPa)
1.00E+00
1.00E+01
1.00E+02
1.00E+03
1.00E+04
1.00E+05
1.00E+06
1.00E+07
1.00E+08
1.00E+09
1.00E+10
Ice crystal number concentration (m-3)
c
Pressure
1
1.05
1.1
1.15
1.2
1.25
1.3
1.35
1.4
Saturation ratio with respect to ice

The decreases of IN concentration in scenarios B and C have the biggest impact on microphysics. This can be seen through the mean ice supersaturation reaching higher values in scenarios B and C than in the reference case A (see Fig. 2c). Ice supersaturation increases in scenarios B and C inasmuch as low IN and ice crystal concentrations reduce the absorption of excess water vapour at the same ice supersaturation. Under these conditions, fewer ice crystals are nucleated than in scenario A. As a result, more water vapour becomes available for growth on fewer ice crystals. Therefore, ice crystals reach larger sizes. This effect is, however, much weaker (a few percent in ice supersaturation) in the more realistic scenario B as compared to scenario C due to much lower sulphuric acid concentration in haze droplets in scenario B.

This process shortens the total water residence time in the lower atmosphere. This effect is seen in the lower 5 km (below 500 hPa) where the total water in the air column (ice crystals plus water vapour) is reduced by as much as 40% in the perturbed simulations. The total water above 5 km is slightly increased due to the increase of specific humidity in scenarios B and C in the upper atmosphere with respect to A. It appears that the decrease of ice water content is compensated by the increase of water vapour.

Fig. 3 shows the total water anomaly as a function of height for scenarios B and C. In the lowest part of the troposphere where ice fog and LLIC occur, the total atmospheric water content in scenarios B and C is 10% to 40% lower than scenario A. This is a clear indication of the effect of a higher dehydration rate of the lower atmosphere in acidic aerosol scenarios. On the other hand, the higher troposphere dehydrates more slowly as the increase of up to 10% of total water in scenarios B and C shows. The lower dehydration above 600 hPa is due to the warming of the upper troposphere in scenario B (see Fig. 4).

The fact that the upper atmosphere is warmer is directly related to the higher dehydration rate of the lower atmosphere. Decreasing the total water in scenarios B and C leads to a reduction of the lower atmosphere midrange emissivity. The strongly saturated

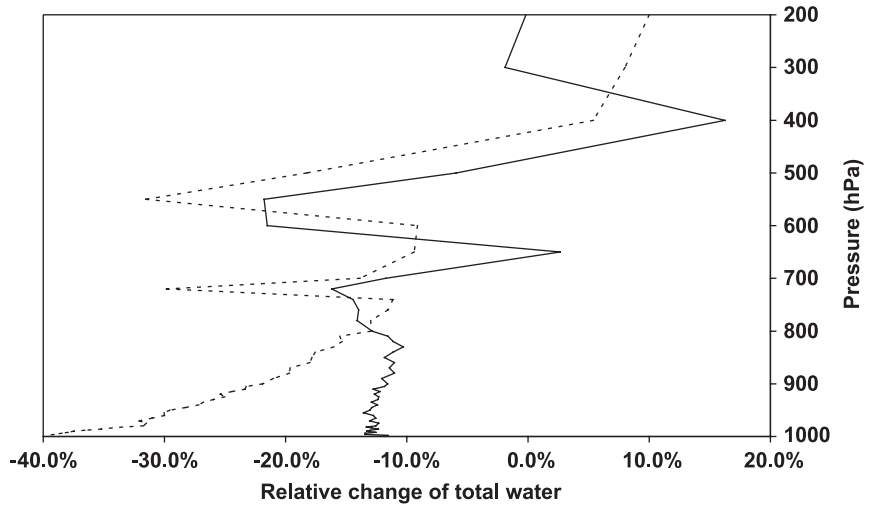

Fig. 3. Vertical profile of the total water anomaly (expressed relatively to the absolute value obtained with aerosol scenario A) averaged over the four cold seasons when scenarios B (full line) and C (dotted line) are considered.

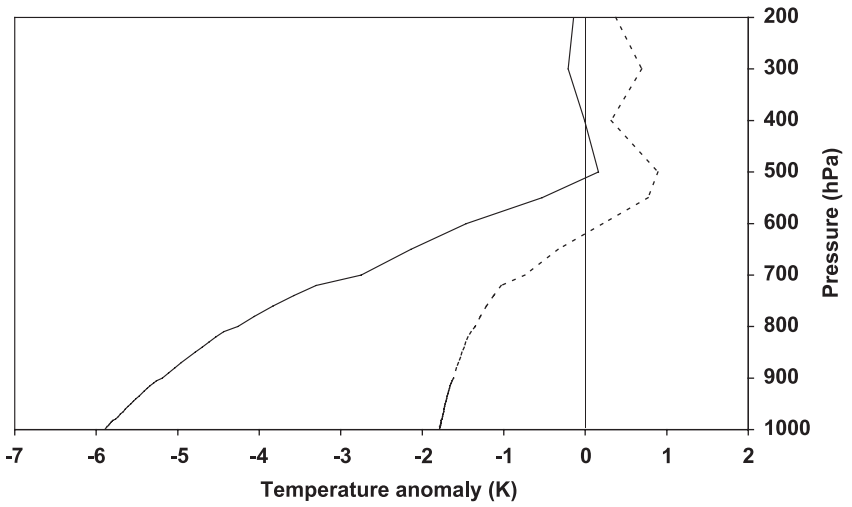

Fig. 4. Vertical profile of the temperature anomaly averaged over the four cold seasons when scenarios B (full line) and C (dotted line) are considered.

region of the infrared spectrum only affects transfer at short vertical distances, while thin windows are mostly transparent in clear layers but often opaque in cloud layers. The infrared radiative flux emitted in intermediate absorption bands by the lower atmosphere decreases, thus reducing the amount of energy transferred to the upper troposphere and the surface. Averaged over the four cold seasons, the reduction of the downward infrared radiation at the surface is 9 and 28 W m^{-2} for scenarios B and C, respectively.

Fig. 4 shows the temperature anomaly produced by the acidification of aerosols averaged over the four cold seasons for scenarios B and C. For scenario B, the surface-based temperature inversion strengthens by 2.7 °C with a cooling of 1.8 °C at the surface and a warming of 0.9 °C at 500 hPa. While the surface cooling is caused by reduced emissivity of the lower atmosphere, as discussed above, the warming at 500 hPa is caused by lower emissivity at this vertical level in scenario B due to reduced cloud amount (see Table 2). Therefore, the cooling rate of this layer in scenario B is also reduced. Inasmuch as the layer 500–1000 hPa is more transparent to infrared radiation coming from the surface, the upwelling infrared flux above 500 hPa increases. Further, the water vapour mixing ratio increases in scenario B and allows for greater infrared radiation absorption in the upper layer, keeping it warmer. In the extreme acidic case (scenario C), the magnitude of the total water decrease in the lower atmosphere leads to a marked diminution of the upward infrared flux to the point that it cannot anymore warm up the upper layers despite a greater amount of total water in these layers. As a result, the mean temperature anomaly is negative throughout the atmosphere with a maximum of −5.8 °C at the surface and a minimum near 0 °C at 500 hPa.

The effect of aerosol acidification on the local climate at Alert shows an important seasonal cycle. Table 3 shows monthly mean values for temperature at two levels, downwelling radiative flux incident to the surface and microphysical properties. These variables are averaged over the 4 years simulated for scenarios A and B. Here, scenario C

Table 3
Monthly mean differences (%) between scenario B and scenario A for temperature, humidity and ice crystal mixing ratio and diameter

	November (%)	December (%)	January (%)	February (%)	March (%)	April (%)	Mean (%)
Surface temperature	0.0	−0.1	−0.5	−1.9	−1.0	−0.3	−0.7
Downwelling infrared radiation	0.1	−0.4	−3.7	−15.2	−10.0	−6.2	−6.3
Specific humidity	0.1	0.4	−5.6	−30.6	−32.5	−4.8	−12.7
Ice mixing ratio	7.6	−17.9	30.2	−22.4	−17.0	−74.6	−25.1
Ice crystal mean diameter	18.8	145.8	31.8	64.2	100.2	51.1	60.0
Total water	0.1	0.3	−5.2	−29.9	−31.8	−4.8	−12.4

is not relevant because the weight fraction of sulphuric acid in aerosol is assumed constant over the whole period. In scenario B, the weight fraction of sulphuric acid is taken from the observation and varies on a weekly basis. As expected, the biggest impact of aerosol acidification occurs during the month with high sulphuric acid ratio. Although the month of April is characterized by the highest concentration of sulphuric acid aerosols during the annual cycle (Sirois and Barrie, 1999), the effect of aerosol acidification appears much smaller compared to February and March. The increased temperature favours higher temperature and SO_2 oxidation. For an effective dehydration–greenhouse feedback, lower temperatures are needed in addition to high acidic aerosol concentration. The two main effects of acidic aerosols are (1) to lower the homogeneous freezing temperature and (2) to decrease the IN concentration. The former effect is active only at low temperatures (<-35 °C). The latter effect is amplified as the temperature decreases due to the nonlinear relationship between active IN concentration and temperature. During autumn, temperatures are relatively low, but the concentration of sulphuric acid aerosol is very low, and the effect of aerosol acidification is small. The optimal conditions occur in February and March with low solar radiation, cold temperature and high sulphuric acid concentration.

4. Observations

Table 4 shows the observed weekly frequency of LLIC and ice fog events as a function of percentage by weight of sulphuric acid to the total aerosol and total sulphate concentrations at Alert for the period of 1991 to 1994. Data from the Alert laboratory station do not provide directly sulphuric acid concentrations (Sirois and Barrie, 1999). Only total sulphate concentration is available. It is generally recognized that the three main components formed by sulphate in the Arctic are ammonium sulphates ($(NH_4)_2SO_4$ and NH_4HSO_4) and sulphuric acid (H_2SO_4) (Sirois and Barrie, 1999). Sulphate is also present

Table 4
Observed frequency of diamond dust and ice fog events as a function of total sulphate mass concentration

	Sulphate>1500 ng/m^3	Sulphate<1500 ng/m^3
Diamond dust	0.20	0.30
Ice fog	0.05	0.01

in the giant aerosol mode mainly in the form of Na_2SO_4 (Seinfeld and Pandis, 1998). However, the number concentration of giant aerosols is very weak in the Arctic during winter (Sirois and Barrie, 1999). The sea ice cover limits local sources of Na_2SO_4. Therefore, most sea salt aerosols reach Alert by long-range transport. Further, cloud processes, wet and dry depositions do not allow for a large concentration of sea salt aerosols to persist in the Arctic during winter (Gong et al., 1997b). Consequently, sulphate mass in the giant mode has been neglected in our analysis.

Under these conditions, using observed ion concentration of NH_4^+ and SO_4^{2-} and assuming only two dominant forms of sulphate, ammonium sulphate and sulphuric acid, the concentration of the latter can be retrieved. The averaged weight fraction of sulphuric acid is 20% of the total aerosol mass. This value was taken as a threshold value for our analysis. Weeks with sulphuric acid ratio higher than 20% are assumed to be associated with high pollution-derived aerosols; otherwise, we consider them to be low pollution-derived aerosols.

Table 4 shows the weekly frequencies of LLIC and ice fog increase in the high pollution-derived aerosols situations. However, the increase of ice fog frequency does not seem to be associated with aerosol acidification but rather to the total sulphate concentration. Indeed, Table 4 shows that when the sulphate concentration is above an averaged value of 1500 ng m^{-3}, ice fog weekly frequency increases by 4% while LLIC weekly frequency decreases by 10%. A priori, inasmuch as a high IN concentration is needed for ice fog formation, the Alert observation appears to be in contradiction with observations about the substantial IN decrease associated with high sulphate concentration (Borys, 1989; Bigg, 1996). One possible explanation is the following. As the mass concentration of sulphate increases, the total aerosol mass also increases, indicating that the concentration of other aerosol types, such as soil particles and organics, likely increases also. In fact, there is a positive correlation of 0.27 and 0.82 between sulphate and soil particle mass concentrations and between sulphate and total aerosol mass concentrations, respectively. Therefore, the increase of ice fog frequency when sulphate and aerosol acidifications are above their average values may not be due to sulphate alone but rather to the increase in concentration of all particle types. In particular, soil particles are excellent IN (Szyrmer and Zawadzki, 1997), and here, they are strongly correlated with sulphate probably due to atmospheric circulation transporting all types of aerosols. Consequently, we cannot rely on aerosol acidification only inasmuch as (1) it is mostly confined to the Aitken mode and (2) few interactions occur by coagulation between Aitken and giant particles due to their large size difference, the small number concentration of giant particles and distinct formation processes.

To isolate the effect of the aerosol acidification and to eliminate as much as possible the influence of other particles like soil particles and some organics, which are likely to be excellent IN, the same analysis was done for one discriminating case: when sulphuric acid mass concentration is above and below its averaged value of 20% for low and high sulphate concentration. Results are shown in Table 5. The case of below average sulphate concentration enables us to capture the aerosol acidification effect for the reasons mentioned above. For this case, the observed weekly frequency of ice fog does not change and the LLIC weekly frequency increases from 27% in low anthropogenic aerosol cases to 43% in high pollution episodes.

Table 5
Observed frequency of diamond dust and ice fog events as a function of total sulphate mass concentration and percentage by weight of sulphuric acid ratio to the total aerosol mass

	H_2SO_4<20%	H_2SO_4>20%
All events	0.25/0.07	0.30/0.15
Sulphate>1500 ng/m^3	0.11/0.03	0.22/0.19
Sulphate<1500 ng/m^3	0.27/0.08	0.43/0.08

The model captures very well the relationship between LLIC frequency and the level of aerosol acidity. LLIC frequency of 39% simulated with scenario C (a high pollution scenario), which corresponds to extreme acidic cases, is close to the mean LLIC frequency observed during high acidic episodes of 43% (that is when sulphuric acid is above its mean value of 20%). Scenario B (realistic lower anthropogenic scenario) with LLIC mean frequency of 23% is also representative of the mean LLIC frequency (for all cases) of 25%.

The observed increase of LLIC weekly frequency is hypothesized to be related to aerosol acidification as follows. LCM simulation has shown that, mostly due to their poor ability to nucleate ice, high pollution-derived aerosols produce fewer ice crystals having larger diameters. The increase of ice crystal mean diameter results in an increase of the ice crystal terminal velocity. As a result, more ice crystals are likely to reach the ground and be reported as an LLIC event in meteorological records.

Such a substantial increase in LLIC frequency can be related to an increase of the air mass dehydration rate and therefore activates the dehydration–greenhouse feedback proposed by Blanchet and Girard (1994, 1995). The same analysis has been done with the LCM output, and results indicate an increase of the LLIC frequency of 10% when the percentage by weight of sulphuric acid is above average. However, model results also indicate a substantial decrease of ice fog frequency that is not observed. The assumption of constant aerosol properties in each scenario is likely to explain some discrepancies. It will be investigated in the next stage of this ongoing research activity. Indeed, large episodic increases of IN concentration were not taken into account in scenario B because of this assumption. Consequently, ice fog frequency was underestimated during peak events.

5. Conclusion

The impact of arctic anthropogenic aerosols dominated by sulphuric acid, on the formation of wintertime lower atmospheric ice crystals and radiation, is evaluated using a single-column model and 4 years of observations at Alert. Two properties related to acidic aerosols are examined to assess their effect on local climate at Alert: (1) the lowering of the homogeneous freezing temperature (for haze droplets) and (2) a lower concentration of IN when the concentration of acidic aerosols increases.

Observations and model simulations corroborate that these properties of wintertime pollution-derived arctic aerosols alter cloud and precipitation physical properties by increasing cloud particle sizes and reducing their number concentration. The weak ability

of anthropogenic acid aerosols to nucleate ice has the most important impact on the behaviour of lower atmospheric ice crystals. One-dimensional simulations at Alert during the period of 1991–1994 showed that the effect of changes in cloud characteristics by aerosol acidification results in larger cloud ice crystals forming in the lower troposphere and more effective LLIC precipitation events. Consequently, we find an increase of the lower troposphere dehydration rate. Radiation calculation with the 1D climate model shows that cloud alteration produces a substantial surface cooling anomaly. If applicable over much of the high Arctic, the impact of acid aerosols on cloud and on surface temperature could explain, at least in part, the cooling tendency in the eastern high Arctic during winter in spite of the CO_2 greenhouse effect and the prediction of GCMs. Further investigations with a full 3D model and more refined simulations are required to assess the complex feedbacks between aerosols, cloud, radiation, sea ice and dynamic transport to further evaluate the impacts of the dehydration–greenhouse feedback on the arctic climate and its regional extent.

Acknowledgments

The authors would like to thank the Canadian Foundation for Climate and Atmospheric Sciences for support funding.

References

Barrie, L.A., 1986. Arctic air pollution: an overview of current knowledge. Atmos. Environ. 20, 643–663.

Bertram, A.K., Patterson, D.D., Sloan, J.J., 1996. Mechanisms and temperature for the freezing of sulphuric acid aerosols measured by FTIR extinction spectroscopy. J. Phys. Chem. 100, 2376–2383.

Bigg, E.K., 1953. The formation of atmospheric ice crystals by the freezing of droplets. Q. J. R. Meteorol. Soc. 79, 510–519.

Bigg, E.K., 1980. Comparison of aerosol at four baseline atmospheric monitoring stations. J. Appl. Metalwork. 19, 521–533.

Bigg, E.K., 1996. Ice forming nuclei in the Arctic. Tellus 48B, 223–233.

Blanchet, J.-P., Girard, E., 1994. Arctic greenhouse cooling. Nature 371, 383.

Blanchet, J.-P., Girard, E., 1995. Water-vapor temperature feedback in the formation of continental arctic air: implications for climate. Sci. Total Environ. 160/161, 793–802.

Blanchet, J.-P., List, R., 1987. On radiative effects of anthropogenic aerosol in arctic haze and snow. Tellus 39B, 293–317.

Borys, R.D., 1989. Studies of ice nucleation by arctic aerosols on AGASP-II. J. Atmos. Chem. 9, 169–185.

Curry, J.A., 1983. On the formation of continental polar air. J. Atmos. Sci. 40, 2278–2292.

Curry, J.A., Meyers, F.G., Radke, L.F., Brock, C.A., Ebert, E.E., 1990. Occurrence and characteristics of lower tropospheric ice crystals in the Arctic. Int. J. Climatol. 10, 749–764.

Curry, J.A., Schramm, J.L., Serreze, M.C., Ebert, E.E., 1995. Water vapor feedback over the Arctic Ocean. J. Geophys. Res. 100, 14223–14229.

Curry, J.A., Rossow, W.B., Randall, D., Schramm, J.L., 1996. Overview of arctic cloud and radiation characteristics. J. Climate 9, 1731–1764.

Cziczo, D.J., Abbatt, J.P.D., 1999. Deliquescence, efflorescence, and supercooling of ammonium sulfate aerosols at low temperature: implications for cirrus cloud formation and aerosol phase in the atmosphere. J. Geophys. Res. 104, 13781–13790.

Girard, E. 1998. Étude d'un effet indirect des aérosols acides en Arctique: le cycle de déshydratation. PhD Thesis, McGill University, 311 p.

Girard, E., Blanchet, J.-P., 2001. Simulation of arctic diamond dust and ice fog and thin stratus using an explicit aerosol-cloud-radiation model. J. Atmos. Sci. 58, 1199–1221.

Girard, E., Blanchet, J.-P., 2001. Microphysical parameterization of arctic diamond dust, ice fog and thin stratus for climate models. J. Atmos. Sci. 58, 1181–1198.

Gong, S.L., Barrie, L.A., Blanchet, J.-P., 1997. Modelling sea-salt aerosols in the atmosphere: 1. Model development. J. Geophys. Res. 102, 3805–3818.

Gong, S.L., Barrie, L.A., Prospero, J.M., Savoie, D.L., Ayers, G.P., Blanchet, J.-P., Spacek, L., 1997. Modelling sea-salt aerosols in the atmosphere: 2. Atmospheric concentrations and fluxes. J. Geophys. Res. 102, 3819–3830.

Heintzenberg, J., 1980. Particle size distribution and optical properties of arctic haze. Tellus 32, 251–260.

Intrieri, J.M., Shupe, M.D., 2004. Characteristics and radiative effects of diamond dust over the western Arctic ocean region. J. Climate 17, 2953–2960.

Koop, T., Ng, H.P., Molina, L.T., Molina, M.J., 1998. Nucleation of ice from H_2SO_4 aerosols. J. Phys. Chem. 102, 8924–8931.

McFarlane, N.A., Boer, G.J., Blanchet, J.-P., Lazare, M., 1992. The Canadian climate center second-generation general circulation model and its equilibrium climate. J. Climate 5, 1013–1044.

Maxwell, J.B., 1982. Climate of the Canadian Arctic islands and adjacent water. Climatol. Stud. 30, 589.

Meyers, M.P., DeMott, P.J., Cotton, W.R., 1992. New primary ice-nucleation parameterization in an explicit cloud model. J. Appl. Metalwork. 31, 708–721.

Pueschel, R.F., Van Valin, C.C., Castillo, R.C., Kadlecek, J.A., Ganor, E., 1986. Aerosol on polluted versus nonpolluted air masses: long range transport and effects on clouds. J. Clim. Appl. Meteorol. 25, 1908–1917.

Radke, R.F., Brock, C.A., Lyons, J.H., Hobbs, P.V., 1989. Aerosol and lidar measurements of hazes in mid-latitude and polar airmasses. Atmos. Environ. 23, 2417–2430.

Randall, D.A., Cripe, D.G., 1999. Alternative methods for specification of observed forcing in single-column models and cloud system models. J. Geophys. Res. 104, 24527–24546.

Rogers, D.C., DeMott, P.J., Kreidenweis, S.M., 2001. Airborne measurements of tropospheric ice-nucleating aerosol particles in the arctic spring. J. Geophys. Res. 106, 15053–15063.

Schnell, R.C., 1984. Arctic haze and the arctic gas and aerosol sampling program (AGASP). Geophys. Res. Lett. 11, 361–364.

Schnell, R.C., Raatz, W.E., 1984. Vertical and horizontal characteristics of arctic haze during AGASP: Alaskan Arctic. Geophys. Res. Lett. 11, 369–372.

Seinfeld, J.H., Pandis, S.N., 1998. Atmospheric Chemistry and Physics: From Air Pollution to Climate Change. John Wiley and Sons. 1326 pp.

Shaw, G.E., 1995. The arctic haze phenomenon. Bull. Am. Meteorol. Soc. 76, 2403–2413.

Sirois, A., Barrie, L.A., 1999. Arctic lower tropospheric aerosol trends and composition at Alert, Canada: 1980–1995. J. Geophys. Res. 104D.

Szyrmer, W., Zawadzki, I., 1997. Biogenic and anthropogenic sources of ice-forming nuclei: a review. Bull. Am. Meteorol. Soc. 78, 209–228.

Trivett, N.B.A., Barrie, L.A., Bottenheim, J.W., Blanchet, J.-P., den Hartog, G., Hoff, R.M., Mickle, R.E., 1988. An experimental investigation of arctic haze at Alert, NWT, March 1985. Atmos.-Ocean 26, 341–376.

Walsh, J.E., Chapman, W.L., 1998. Arctic cloud–radiation–temperature associations in observational data and atmospheric reanalyses. J. Climate 11, 3030–3045.

Wexler, H., 1936. Cooling in the lower atmosphere and the structure of polar continental air. Mon. Weather Rev. 64, 122–136.

Witt, H.J., 1968. Airborne observations of cloud particles and infrared flux density in the Arctic. MS thesis, Dept. of Atmospheric Sciences, University of Washington.

Yli-Tuomi, T., Vanditte, L., Hopke, P.K., Shamasuzzoha Basunia, M., Landsberger, S., Viisanen, Y., Paatero, J., 2003. Composition of the Finnish Arctic aerosol: collection and analysis of historic filter samples. Atmos. Environ. 37, 2355–2364.